remote sensing

MDPI

Communication

HIRS Outgoing Longwave Radiation—Daily Climate Data Record: Application toward Identifying Tropical Subseasonal Variability

Carl J. Schreck III [1,*], Hai-Tien Lee [2] and Kenneth R. Knapp [3]

[1] North Carolina Institute for Climate Studies (NCICS)/Cooperative Institute for Climate and Satellites—NC (CICS-NC), North Carolina State University, Asheville, NC 28801, USA
[2] Earth System Science Interdisciplinary Center (ESSIC)/Cooperative Institute for Climate and Satellites—MD (CICS-MD), University of Maryland, College Park, MD 20740, USA; lee@umd.edu
[3] NOAA's National Centers for Environmental Information (NCEI), Asheville, NC 28801, USA; ken.knapp@noaa.gov
* Correspondence: cjschrec@ncsu.edu; Tel.: +1-828-257-3140

Received: 21 June 2018; Accepted: 17 August 2018; Published: 21 August 2018

Abstract: This study describes the development of a new globally gridded climate data record (CDR) for daily outgoing longwave radiation (OLR) using the High-Resolution Infrared Radiation Sounder (HIRS) sensor. The new product, hereafter referred to as HIRS OLR, has several differences and advantages over the widely-used daily OLR dataset derived from the Advanced Very High-Resolution Radiometer (AVHRR) sensor on the same NOAA Polar Operational Environmental Satellites (POES), hereafter AVHRR OLR. As a CDR, HIRS OLR has been intersatellite-calibrated to provide the most homogeneous record possible. AVHRR OLR only used the daytime and nighttime overpasses from a single satellite at a time, which creates some challenges for resolving the large diurnal cycle of OLR. HIRS OLR leverages all available overpasses and then calibrates geostationary estimates of OLR to represent that cycle more faithfully. HIRS also has more spectral channels, including those for measuring water vapor, which provides a more accurate measure of OLR. This difference is particularly relevant for large-scale convective systems such as the El Niño–Southern Oscillation and the Madden–Julian Oscillation, whereby the HIRS OLR can better identify the subtropical variability between the tropical convection and the extratropical teleconnections.

Keywords: climate data record; outgoing longwave radiation; Madden–Julian Oscillation; tropical waves

1. Introduction

Outgoing longwave radiation (OLR) is one of the World Meteorological Organization's (WMO's) essential climate variables and is a key component of the earth's radiation budget. OLR is also a critical proxy for tropical convection. In clear regions, OLR values are high in association with the emissions from the hot tropical surface. In cloudy regions, OLR is related to the cloud-top temperature, with higher clouds producing lower values of OLR. That relationship makes OLR a viable proxy for convection and even precipitation in the tropics, since more vigorous convection produces taller clouds with colder tops and thus lower OLR.

Liebmann and Smith [1] developed a daily OLR product in 1996, based on the NOAA National Environmental Satellite, Data, and Information Service (NESDIS) operational OLR product [2], that used the Advanced Very High Resolution Radiometer (AVHRR) sensor on the NOAA Polar Operational Environmental Satellites (POES). These satellites are sun-synchronous, so they see most points on earth twice a day through the course of 14 orbits. Liebmann and Smith used the afternoon (1430) satellite

when available. Gaps in coverage were filled through an iterative spatiotemporal interpolation scheme. Because of the strong diurnal cycle of OLR, the daytime and nighttime overpasses were interpolated separately, and then the resulting complete grids were averaged together. The data were provided on a daily 2.5° global grid with complete coverage from 1979 to the present. This dataset will be referred to hereafter as AVHRR OLR.

The AVHRR OLR was one of the first available globally complete gridded proxies for daily clouds or rainfall. As a result, Liebmann and Smith's [1] short 3-page paper has been cited over 1500 times. Many of those citations use it to identify tropical convective variability. A landmark paper by Wheeler and Kiladis [3] calculated the zonal wavenumber–frequency power spectrum of AVHRR OLR and showed that many of the peaks in spectral power occur along dispersion curves for linear shallow water equatorial waves [4,5]. Another large peak was associated with the Madden–Julian Oscillation (MJO) [6], the dominant mode of subseasonal variability in the tropics. The MJO was first discovered in the spectral analysis of zonal wind data in tropical radiosondes [7], but its close association with convection was shown soon thereafter [8]. As a result, the industry standard for identifying and tracking the MJO, the Real-time Multivariate MJO (RMM) index [9], uses a combination of zonal winds and AVHRR OLR.

This paper describes a new daily gridded OLR dataset that was recently developed as part of NOAA's Climate Data Record Program. The new dataset uses a different sensor, the High-Resolution Infrared Radiation Sounder (HIRS), on the same NOAA POES satellites. HIRS produces a more accurate estimate of OLR by using more spectral channels that provide vertical structure information on the atmospheric temperature and water vapor in addition to the surface/cloud-top emission, whereas the AVHRR OLR retrieval depends solely on the surface/cloud-top emission information. Like many atmospheric observing platforms, the NOAA POES sensors were designed and maintained to support weather forecasting, which means they may not be ideal for climate analysis [10]. Both AVHRR and HIRS have evolved over the generations of satellites, yet even sensors designed on the ground to be identical may produce different results once in orbit. The original AVHRR did not account for these difference or other non-climatic changes such as shifts in the overpass time between satellites or even over the course of one satellite's lifetime.

The new dataset, referred to hereafter as HIRS OLR, addresses many of the issues described above. Intersatellite calibration produces a more homogeneous record. It uses all available NOAA POES and MetOp satellites to maximize the coverage, and geostationary estimates of OLR are calibrated to the HIRS values to improve the fidelity of the diurnal cycle. In addition to these algorithmic changes, the HIRS sensor is sensitive to water vapor, which gives a more robust estimate of the OLR and the associated variations in tropical convection.

2. Materials and Methods

The multi-spectral OLR estimation method was developed by Ellingson et al. [11] and uses narrowband radiance observations from the High-Resolution Infrared Sounder (HIRS) to estimate TOA total longwave flux. Vigorous validation efforts were performed for the HIRS OLR estimation technique against broadband observations derived from the Earth Radiation Budget Experiment (ERBE) and the Clouds and the Earth's Radiant Energy System (CERES) [12,13]. Details of the HIRS sensor can be found in the NOAA Polar Orbiter Data (POD) User's Guide [14], the NOAA KLM User's Guide [15], and the C-ATBD for the HIRS OLR climate data record (CDR) [16].

The multi-spectral OLR estimation technique has been adapted successfully to the Geostationary Operational Environmental Satellite (GOES)-Sounder [17] and GOES-Imager instruments [18]. These studies have shown that this OLR estimation algorithm can reliably achieve an accuracy of about 4–8 W m^{-2} for various instrument types, with biases (precision) that are within the respective radiometric accuracy of the reference instruments. The HIRS OLR algorithm has been implemented to generate the NESDIS operational HIRS OLR product since September 1998, and the OLR products retrieved from operational geostationary satellites are implemented as part of the operational GOES

Surface and Insolation Product (GSIP) [19]. A variant of this method has been developed for the GOES-R Advanced Baseline Imager instrument [20].

The main components of the HIRS OLR algorithm include the HIRS radiance calibration, OLR retrievals (polar-orbiting HIRS and geostationary imagers), the HIRS/Imager OLR blending procedure, and the temporal integration that determines the daily mean OLR at each $1^\circ \times 1^\circ$ grid box.

The OLR diurnal variation is explicitly resolved with geostationary satellite observations. The GridSat CDR product [21] provides the inter-calibrated and limb-corrected brightness temperatures for window and water vapor channels. The GridSat OLR is estimated with an algorithm adapted from the AVHRR OLR algorithm [2]. In addition to the Imager Window channel observations, the water vapor channel observations are also used to increase accuracy. The GridSat OLR is calibrated against the HIRS OLR retrievals to remove regional biases and to maintain absolute radiometric accuracy [18].

The HIRS/Imager OLR blending procedure performs the inter-calibration of the HIRS and Imager OLR, the temporal interpolation for missing data (e.g., for orbital gaps over the tropics), and the daily integral. This is carried out over a "7-day boxcar" for each of the $1^\circ \times 1^\circ$ grid boxes, where the "7-day boxcar" is a moving boxcar unit spanning 7 days, centered on the target day. The length of the moving boxcar is chosen because the estimation errors in the Imager OLR mainly originate from deficiencies in water vapor variation information. The boxcar needs to be short enough to identify the transient variations but long enough to provide sufficient data for reliable calibration. For the spatial aspect, the calibration is performed over each one-degree grid box opposed to the full disk scope such that regional and scene-dependent Imager OLR bias errors can be determined. The application of the moving boxcar at each grid box enables the inter-calibration procedure to remove Imager OLR biases localized in both space and time, while maintaining continuity in the bias adjustment.

The HIRS OLR production uses multi-platform observations that require critical data merging techniques to achieve consistency and continuity. The critical components are the OLR retrieval and the temporal integral.

2.1. OLR Retrieval

Obtaining consistent OLR retrievals from all satellites is achieved through two controlling factors: (1) consistent OLR regression models and (2) inter-satellite calibration.

The coefficients for OLR regression models are satellite/instrument-specific. Since the coefficients are derived from a common set of simulations, the OLR regression models for different satellites and instruments would have consistent error characteristics if the instruments were not changed. However, due to the variations in channel specifications for HIRS-2, 2I, 3 and 4, the modification of the OLR regression model formulation is necessary, but this results in inconsistencies in their regression error characteristics. These in turn interfere with inter-satellite calibration procedure and reduce the robustness of the inter-satellite calibration results. The new v2.7 OLR models use radiance observations available to all versions of HIRS instruments that significantly improved the consistency of OLR retrievals and the accuracy of the inter-satellite calibrations [22]. By contrast, the OLR regression models used in the NOAA NESDIS Operational HIRS OLR production were optimized for individual versions of the HIRS instruments, without considering the time series continuity.

The inclusion of extra opaque high cloud in the radiation simulation datasets extends OLR samples in the low-end range. The OLR regression residual behavior is much improved when the non-linear radiance predictor terms are included. The combined effect is the elimination of biases at the high and low end of OLR values, particularly for the low end. The consistency in the residual behavior between OLR models and the removal of low-end biases helps to secure the inter-satellite calibration that primarily relies on polar data due to collocation limitations.

2.2. Temporal Integral

Sun-synchronous polar orbiters have low temporal sampling rate: twice a day for each satellite for the tropics and midlatitudes. The daily OLR can err by as much as 100 W m^{-2} locally if diurnal

variation is not accounted for accurately. However, the daily diurnal variation is too transient to be described by static diurnal models. The geostationary observations, with a 15-min to 3-hourly refresh rate over full disk domains, can be used to provide the OLR diurnal variation information needed for accurate daily OLR determination.

The atmospheric window channel is common to the Imager instruments aboard all geostationary satellites, while some have a 6.7 μm water vapor channel [23]. We can estimate OLR from these observations, although with uncertainties about 3 to 4 times larger than those of HIRS OLR retrievals because of the lack of atmospheric vertical structure information in Imager observations.

A blending procedure merges HIRS/Imager OLR data for the daily OLR determination. Since the HIRS OLR retrieval has higher precision and is considered as the absolute radiometric reference, the Imager OLR is adjusted towards the HIRS OLR within a processing unit termed "7-day boxcar" on the grid-by-grid basis (Figure 1).

The blending procedure involves the following steps:

1. HIRS OLR (Figure 1, red points) is gridded as hourly data time stamped at the middle of the hour; Imager OLR (Figure 1, black stars) is gridded as 3-hourly data, stamped at the nominal hours, 00Z, 03Z, . . . , 21Z;
2. Seven-day boxcar data is constructed with HIRS and Imager OLR data;
3. Inter-calibration for HIRS OLR is applied, with average HIRS OLR if observations occupy the same hour box;
4. The Imager OLR (spline) is interpolated to hourly bins and coincident HIRS/Imager pairs are constructed for use in Imager to HIRS calibration;
5. Linear regression is generally used to calibrate the Imager to HIRS. However, it may not always yield reliable results, e.g., when the OLR variance is low (leads to poor signal to noise ratio), or when the fitting has relatively low confidence. To avoid introducing a faulty calibration, a straight offset (i.e., forced with slope one) is applied for any of the following scenarios:

    a. HIRS OLR variance is too small (STD < 20 W m^{-2});
    b. The explained variance by the linear regression is less than 50%;
    c. When the number of data points of calibration pairs is less than 7.

6. The Imager OLR data is adjusted (Figure 1, blue diamonds) and now reaches the same absolute radiometric level as in HIRS;
7. Imager OLR is combined with HIRS OLR to form a single hourly time series (Figure 1, red curve);
8. Trapezoidal rules are applied over all available data (at a 3-hourly or better sampling rate) to derive the integral for the target day. The target day is the center (4th day) of the 7-day boxcar (Figure 1, green vertical lines).

This process effectively removes scene-dependent biases in the Imager OLR retrievals. The 7-day temporal window provides a sufficient number of coincident samples for Imager-to-HIRS calibration while keeping the origins of the biases locally in both space and time (e.g., water vapor variation). It also allows the estimation of a daily mean when HIRS is not available (e.g., due to orbital gap or missing orbits) on the target day, once the imager OLR data and its calibration information are available. This procedure essentially eliminates the need for spatial filling for orbital gaps, which can cause relatively large errors even with the optimum interpolation method. The daily temporal integral can then be accurately determined with all the available OLR data, the HIRS and the calibrated Imager OLR, at a 3-hourly or better temporal sampling interval.

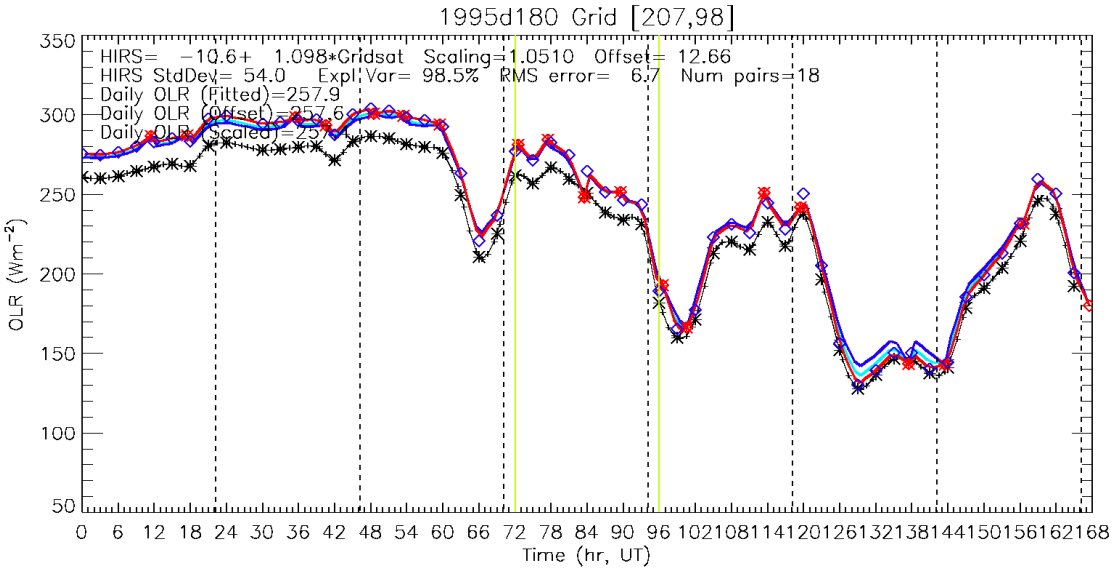

Figure 1. Example 7-day boxcar for day 180 of year 1995 on the grid cell [207, 98]. The Imager outgoing longwave radiation (OLR) (black stars) is calibrated against the High-Resolution Infrared Radiation Sounder (HIRS) OLR (red points). The calibrated Imager OLR (blue diamonds) is obtained through the linear function determined by the regression on the coincident HIRS/Imager OLR pairs. The dashed vertical black lines indicate solar noons, while the two green vertical lines delineate the target day (in UTC) for the daily average OLR derivation. The daily OLR for the target day (between the two green lines) is derived with trapezoidal rule applying to all OLR data, including the HIRS OLR and the calibrated Imager OLR data. To visualize the temporal integration, the red curve indicates the OLR variation described with combined HIRS and Imager OLR, after the Imager OLR is linear adjusted. The blue curve represents that when the imager OLR is adjusted only by the Offset, while the cyan curve represents that when the Imager OLR is adjusted by the scaling method (which is not used in this algorithm). The impact of the Imager OLR calibration can be seen as the gap between the black curve (connecting the original Imager OLR data points) and the red curve, with the latter represents the "best estimate" of the OLR diurnal variations with the blending technique.

3. Results

3.1. Validation

Figure 2 compares the HIRS OLR with CERES OLR estimates from the CERES EBAF (energy balance and filled) Ed2.6r and SYN1deg-day Ed3A products. The CERES EBAF product provides monthly averages of top of the atmosphere radiative fluxes at 1° × 1° resolution. The CERES SYN1deg product, also at 1° × 1° resolution, incorporates radiative fluxes estimated by Imager observations on geostationary satellites to improve temporal integration accuracy for the diurnal variations. The validation against CERES is limited to March 2000 and onward. The results shown here contain data between March 2000 and December 2012, as the validation campaign was performed in 2014. The HIRS daily OLR CDR dataset provides global coverage from 1 January 1979 to the present, but with some missing days, mostly in 1985, due to HIRS instrument malfunctions on the NOAA-9 satellite.

Global anomalies are shown on the left (Figure 2a,c), and the tropical (20°S–20°N) anomalies are shown on the right (Figure 2b,d). The top row (Figure 2a,b) compares monthly averages of the HIRS OLR with the CERES EBAF OLR product. Similarly, the bottom row (Figure 2c,d) compares the daily values of HIRS OLR with the CERES SYN1deg OLR product. The OLR anomalies (blue and red curves) show strong agreement on both timing and amplitude of the variability between the two products. The difference curves (green) confirm that agreement. The trends of the OLR anomaly differences

for the global and the tropical domains are 0.03 ± 0.09 W m^{-2} per decade and 0.28 ± 0.10 W m^{-2} per decade, respectively, at 2-sigma level, which satisfies the stability requirement for climate quality data: ±0.3 W m^{-2} per decade [2]. Disagreements between HIRS and CERES daily OLR were relatively larger in the 2000–2002 pre-Aqua (TERRA-only) period. This is due to the limitation in the number of observations that were available to the CERES daily OLR. The standard deviations of the differences of the two products clearly demonstrate this effect (see Figure 10b in [16]).

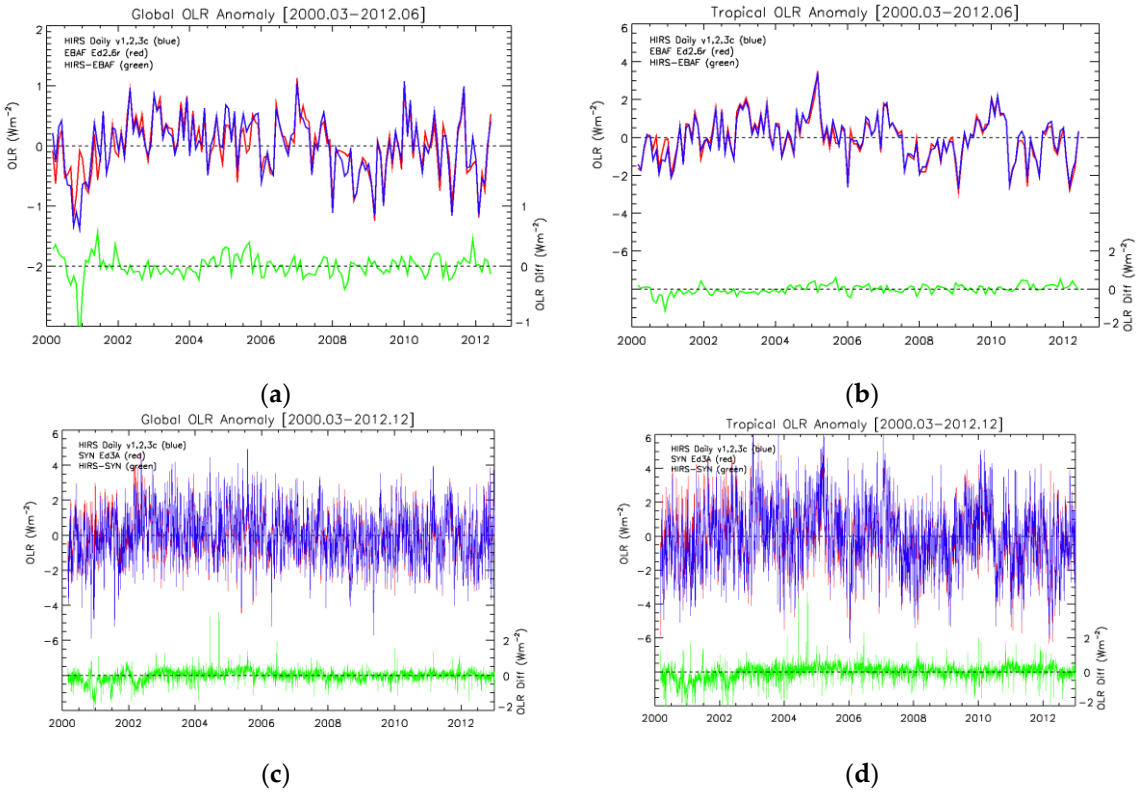

Figure 2. Top: Comparison of monthly OLR anomalies between the daily OLR climate data record (CDR) (blue) and the Clouds and the Earth's Radiant Energy System (CERES) energy balance and filled (EBAF) OLR product (red) over the (**a**) global and (**b**) tropical 20S-20N domains. Bottom: Comparison of daily OLR between the daily OLR CDR (blue) and the CERES SYN1deg OLR product (red) over the (**c**) global and (**d**) tropical 20S–20N domains for the 2000–2012 period. The green curves are for their differences. The y-axes are (**a**) −3 to + 2 W m^{-2}, and (**b**–**d**) −7 to + 5 W m^{-2}.

3.2. Comparison

Figure 3 shows the 1981–2010 climatological differences in mean and variance of the HIRS and AVHRR OLR datasets (contours) overlaid with the HIRS values (contours). The difference is calculated by interpolating the 1.0° HIRS OLR data onto the same grid as the 2.5° AVHRR OLR. As may be expected, both the mean and variance are largely driven by differences between the intense convection in the monsoons and ITCZ regions compared with the drier subtropical subsidence zones. The mean OLR is lowest in regions of deep clouds, which have much colder tops than the warm land and ocean below. Variance is the opposite. Convection naturally has a large degree of variability, and this is accentuated by the large differences in OLR between the intermittent clear and cloudy periods at any given point.

HIRS generally has higher values of OLR, especially in the subtropics, as indicated by the red shading. These differences are primarily driven by the scene-dependent biases in AVHRR OLR retrieval and the differences in radiometric calibration references adopted by the two algorithms. Meanwhile, HIRS has lower variance within the convective regions. This difference likely relates to the inclusion of

a water vapor channel in the HIRS sensors. The decreased OLR from humid columns of air provides some intermediary values between clear and cloudy conditions. On the other hand, the variance is more similar between the two datasets in the subtropical subsidence regions. Here, the typical lack of clouds would hamper the variability in AVHRR OLR, while HIRS may be able to detect water vapor signatures from variations in the strength of that subsidence.

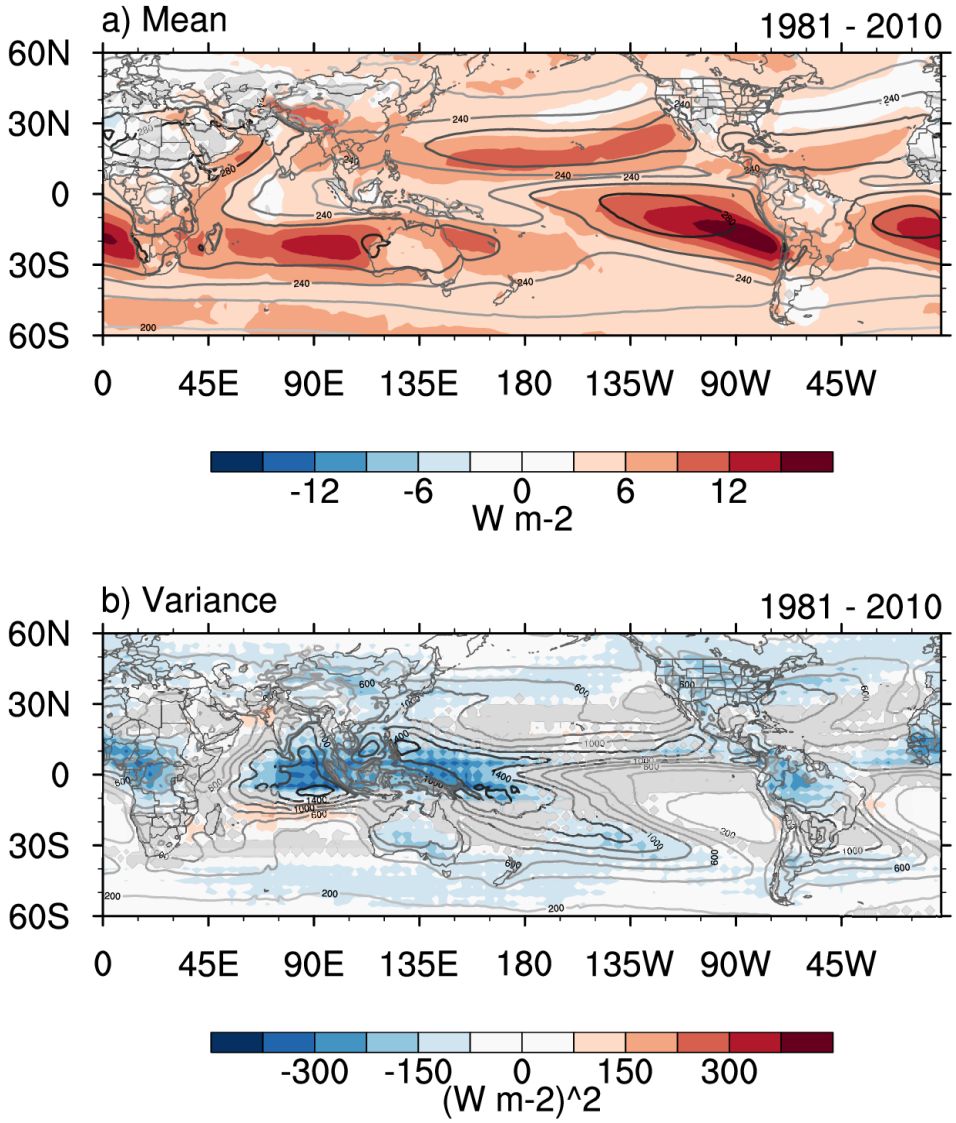

Figure 3. Comparison of mean (**a**) and daily variance (**b**) between HIRS and Advanced Very High-Resolution Radiometer (AVHRR) OLR. The difference is shaded and the HIRS average is contoured. Gray shading masks regions where the differences are not statistically significant at the 95% level.

Figure 4 shows these differences with histograms comparing collocated HIRS and AVHRR data for various latitude bands. Consistent with Figure 3a, HIRS generally has higher values of OLR than AVHRR, hence most of the data falls to the right of the diagonal (black line). The relationships are somewhat nonlinear, however, with a stronger bias at the higher (>250 W m^{-2}) and lower values (<200 W m^{-2}). The bias also varies with latitude. It is most pronounced for higher values in the tropics (20°S–20°N) and subtropics (20–40°), particularly in the Southern Hemisphere. These differences are caused by the retrieval biases in AVHRR OLR, which is known to be too low within the trade wind inversions in the tropics [24]. AVHRR's insensitivity to water vapor leads to the incorrect accounting of its effect on OLR. The bias is also larger for lower OLR values at higher latitudes (40°–90°), especially

in the Southern Hemisphere because of the discontinuity between earth surface and air temperatures over the cold and dry Antarctica (especially during the night time). This discontinuity misleads the window-channel-only AVHRR algorithm to produce too low OLR estimates [24].

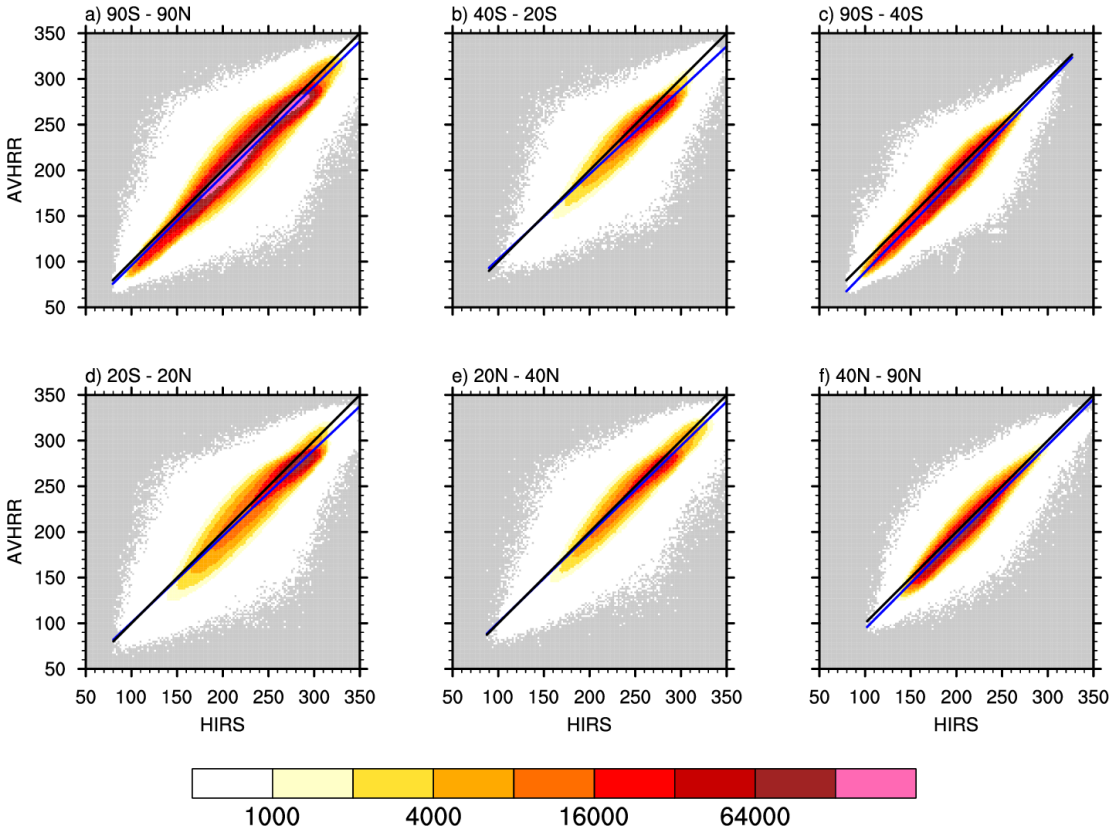

Figure 4. Histogram comparing collocated HIRS and AVHRR data for various latitude bands: (**a**) global (90°S–90°N); (**b**) Southern Hemisphere subtropics (40°S–20°S); (**c**) Southern Hemisphere extratropics (90°S–40°S); (**d**) equatorial strip (20°S–20°N); (**e**) Northern Hemisphere subtropics (20°N–40°N); and (**f**) Northern Hemisphere extratropics (40°N–90°N). The black diagonal indicates the one-to-one line, while the blue diagonal is the linear best fit. Gray shading indicates zero.

One popular application of OLR data has been in identifying the MJO and equatorial waves [3,25,26]. Figure 5 shows the differences in the zonal wavenumber–frequency spectra between HIRS and AVHRR OLR. The spectrum of OLR is generally red, with the highest power at lower frequencies and wavenumbers (Figure 5, top row, contours). HIRS is even redder with somewhat higher power at low frequencies and wavenumbers and less power at smaller scales. These differences are generally not statistically significant (gray shading) except for some of the reduction of small-scale power for the component of the signal that is anti-symmetric about the equator (Figure 5, top left).

Wheeler and Kiladis [3] showed that dividing these spectra by a smoothed estimate of the red background highlighted these modes more clearly. The contours in the bottom row of Figure 5 show the resulting normalized power for HIRS OLR, while the shading shows differences between the normalized spectra for the two datasets. Similar to the total spectral power (Figure 5, top row), AVHRR has somewhat stronger power at the lower frequencies and wavenumbers associated with the MJO and convectively coupled equatorial Rossby (ER) waves. However, these differences are again not statistically significant. As in the total spectra, the normalized spectra show a small but statistically significant difference in the anti-symmetric spectrum for periods less than 2.5 days and eastward propagating wavenumbers higher than 10.

The largest difference between the spectra for AVHRR and HIRS occurs with a period around 9 days and an eastward propagating wavenumber of 14. This power relates to a known spurious signal in the AVHRR data caused by the satellites' orbital precession projecting onto the diurnal cycle. The HIRS OLR dataset eliminates this issue by using geostationary GridSat data to more faithfully resolve the diurnal cycle.

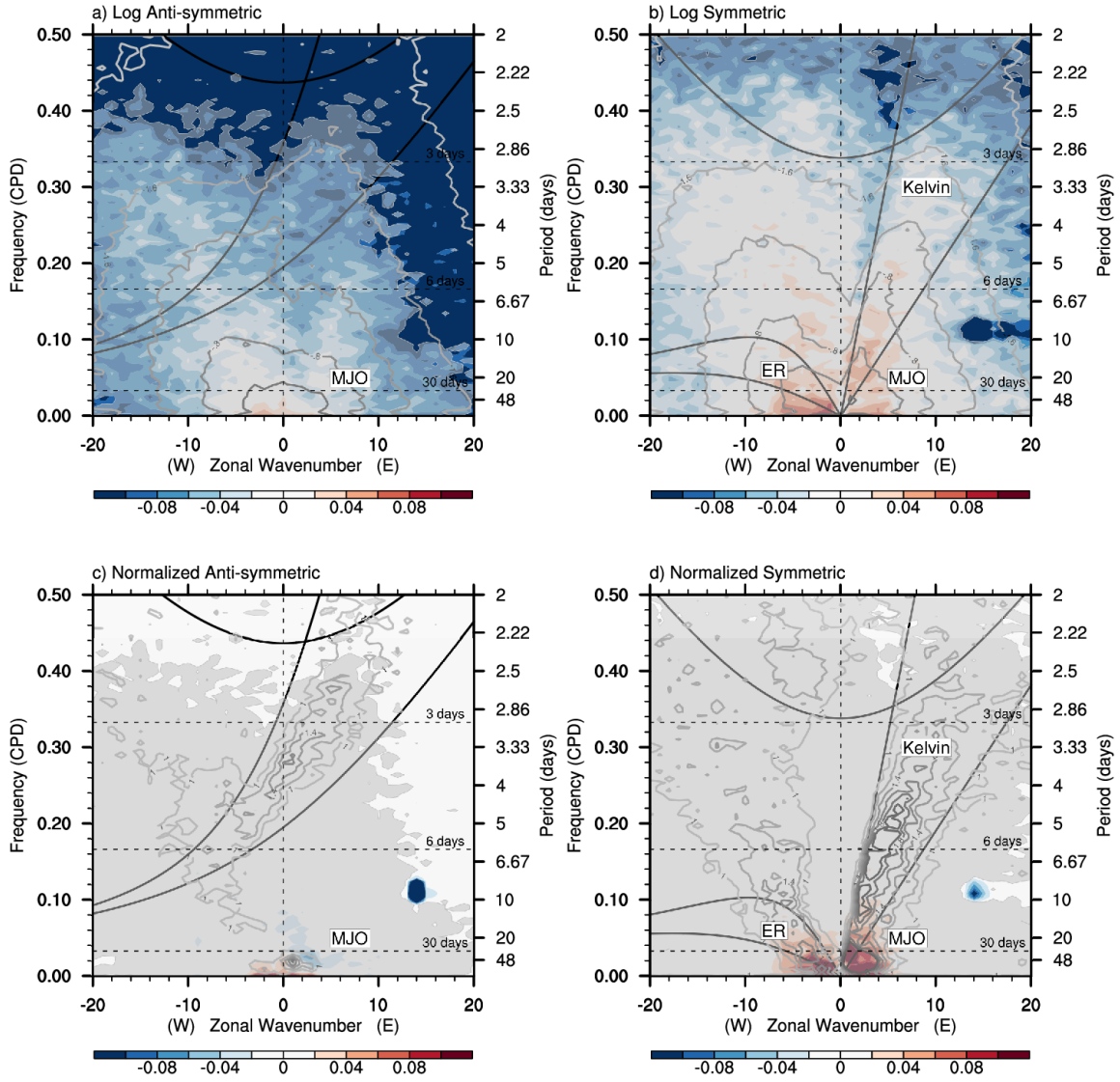

Figure 5. Differences between the zonal wavenumber–frequency power spectra for (**a**,**c**) anti-symmetric about the equator, (**b**,**d**) symmetric about the equator, (**a**,**b**) total power and (**c**,**d**) normalized by the red background. Shading indicates the difference between HIRS and AVHRR and contours indicate the values for HIRS. Gray shading masks regions where the differences are not statistically significant at the 95% level. Black lines denote the theoretical shallow water dispersion curves for various equatorial waves [4,5].

Figure 6 compares the geographic distribution of wave-filtered variance for four of the key subseasonal-to-seasonal tropical modes: low-frequency variability with periods longer than 120 days often associated with ENSO, the MJO, convectively coupled atmospheric Kelvin waves, and convectively coupled equatorial Rossby (ER) waves. Low-frequency variability (Figure 6a) is naturally maximized with ENSO in the equatorial Pacific. The differences are primarily in the subtropical regions, particularly those flanking the equatorial Pacific, where HIRS has more variability than AVHRR. This

difference is again not surprising since HIRS is sensitive to variations in water vapor in these generally cloud-free subsidence regions. The MJO map is similar (Figure 6b). The variability is enhanced in the Indo–Pacific warm pool, but the differences are largest in the subtropical regions. The MJO has substantial interactions with the extratropical circulation, and HIRS ability to identify MJO variability in these transition regions may improve the identification of those interactions [27].

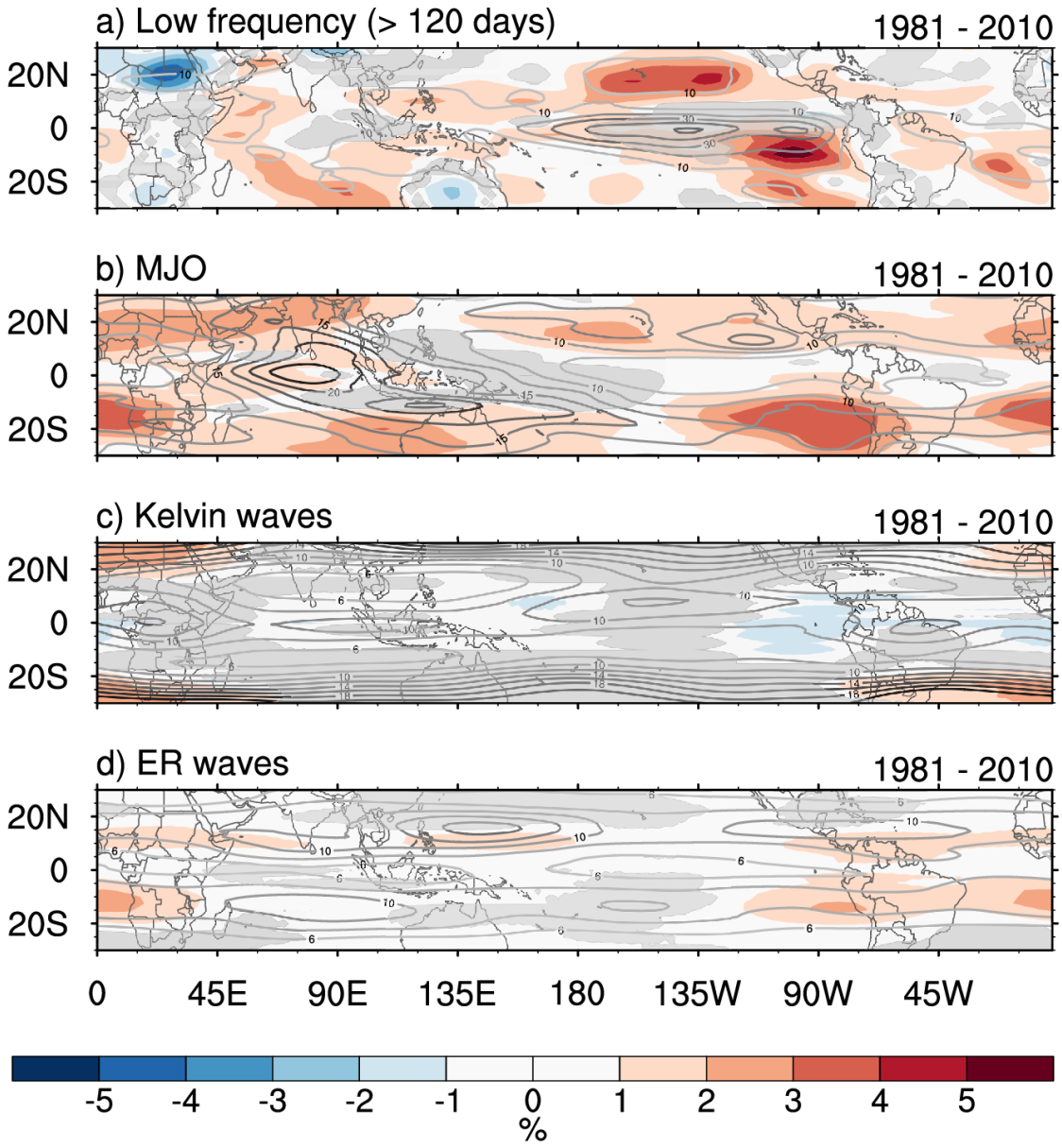

Figure 6. Variance for each tropical subseasonal mode (contours) and the difference between HIRS and AVHRR (shading). (**a**) Low-frequency, (**b**) MJO, (**c**) Kelvin waves, and (**d**) ER waves. Gray shading masks regions where the differences are not statistically significant at the 95% level.

The differences between HIRS and AVHRR are subtler for Kelvin and ER waves (Figure 6c,d). Kelvin variance maximizes in the ITCZ regions. However, these waves move eastward with roughly the same scale and eastward phase speed as extratropical Rossby waves. The Kelvin filter cannot distinguish these systems in OLR, so the Kelvin variance actually increases in the extratropics. The overall differences in variance are small between the two sensors, however. AVHRR has a little more Kelvin signal over the eastern Pacific and tropical Atlantic, while HIRS has more associated

with extratropical systems near Africa. ER waves are unique in that their variance peaks off the equator near 20° latitude. The differences are again small, but HIRS has somewhat more power than AVHRR.

4. Conclusions

This manuscript describes a new CDR for daily OLR from the HIRS sensors. This dataset is compared with the previous industry standard, the AVHRR OLR from NOAA ESRL and CPC [1]. Both datasets use sensors on the sun-synchronous NOAA and MetOp polar orbiting satellites. However, they have several key differences both in the sensors' uses and in how the data are processed.

Both the AVHRR and HIRS sensors have evolved somewhat over the nearly 40 years of the NOAA POESS series. Even sensors designed identically cannot avoid some variance in their actual measurements. For these reasons, the HIRS OLR CDR includes intersatellite calibration to produce a climate-quality homogenous dataset.

The AVHRR OLR exclusively uses the twice-daily overpasses from one satellite at a time. The strong diurnal cycle of tropical convection poses a challenge to producing a representative daily average from these satellites. It also leads to the orbital precession of the satellite aliasing onto the AVHRR OLR spectra (Figure 5). The new HIRS OLR CDR confronts these challenges by calibrating geostationary OLR estimates using the HIRS data and then using the daily average of the combined time series. This method also eliminates the need to interpolate gaps between overpasses, as these are instead filled with the calibrated geostationary data.

The most significant difference is in how OLR is calculated from each sensor. HIRS has water vapor channels that AVHRR does not. That means AVHRR is primarily sensitive to the temperature at the top of the clouds or at the surface in clear columns. Since water vapor is an important greenhouse gas, HIRS provides a much more accurate representation of the radiation budget. The inclusion of water vapor also has important implications for identifying tropical convection. AVHRR can essentially only see clear or cloudy, but HIRS can distinguish between moist and dry clear columns. This difference is particularly important in the subtropical subsidence regions.

The differences in the subtropics are particularly strong for the two primary modes of tropical subseasonal-to-seasonal variability: the MJO and ENSO (Figure 6). The variations with ENSO play a significant role in the interannual global radiation budget [28]. For the MJO, the subtropical variability can be a critical bridge between the tropical convection and its extratropical impacts [27]. Ongoing research is investigating how best to leverage these signals to improve subseasonal-to-seasonal forecasts for extratropical teleconnections.

The archive of the daily OLR CDR v1.2 data sets in NetCDF4 format—spanning from 1 January 1979 to the present (doi:10.7289/V5SJ1HH2) [29], its technical documentation (C-ATBD) [16], and the associated production source codes and ancillary data—are publicly available at the NOAA NCEI CDR Program web site: https://www.ncdc.noaa.gov/cdr/atmospheric/outgoing-longwave-radiation-daily. The near real-time update of the daily OLR CDR product can be found at http://olr.umd.edu.

Author Contributions: Conceptualization, C.J.S.III, H.-T.L., K.R.K.; Methodology, H.-T.L.; C.J.S.III wrote the paper with input from co-authors. All of the authors contributed to the paper through their review, editing, and comments.

Funding: This work was supported by NOAA through the Cooperative Institute for Climate and Satellites—North Carolina State University and University of Maryland College Park under Cooperative Agreement NA14NES432003.

Acknowledgments: The authors thank Anand Inamdar and four reviewers for insightful comments on the manuscript.

Conflicts of Interest: The authors declare no conflict of interest. The funders had no role in the design of the study; in the collection, analyses, or interpretation of data; in the writing of the manuscript, and in the decision to publish the results.

References

1. Liebmann, B.; Smith, C.A. Description of a complete (interpolated) outgoing longwave radiation dataset. *Bull. Am. Meteorol. Soc.* **1996**, *77*, 1275–1277.
2. Ohring, G.; Gruber, A.; Ellingson, R. Satellite determinations of the relationship between total longwave radiation flux and infrared window radiance. *J. Climatol. Appl. Meteorol.* **1984**, *23*, 416–425. [CrossRef]
3. Wheeler, M.; Kiladis, G.N. Convectively coupled equatorial waves: Analysis of clouds and temperature in the wavenumber–frequency domain. *J. Atmos. Sci.* **1999**, *56*, 374–399. [CrossRef]
4. Matsuno, T. Quasi-geostrophic motions in the equatorial area. *J. Meteorol. Soc. Jpn. Ser. II* **1966**, *44*, 25–43. [CrossRef]
5. Lindzen, R.D. Planetary waves on beta-planes. *Mon. Weather. Rev.* **1967**, *95*, 441–451. [CrossRef]
6. Zhang, C. Madden-julian oscillation. *Rev. Geophys.* **2005**, *43*, RG2003. [CrossRef]
7. Madden, R.A.; Julian, P.R. Detection of a 40–50 day oscillation in the zonal wind in the tropical Pacific. *J. Atmos. Sci.* **1971**, *28*, 702–708. [CrossRef]
8. Madden, R.A.; Julian, P.R. Description of global-scale circulation cells in the tropics with a 40–50 day period. *J. Atmos. Sci.* **1972**, *29*, 1109–1123. [CrossRef]
9. Wheeler, M.C.; Hendon, H.H. An all-season real-time multivariate MJO index: Development of an index for monitoring and prediction. *Mon. Weather Rev.* **2004**, *132*, 1917–1932. [CrossRef]
10. National Research Council. *Climate Data Records from Environmental Satellites: Interim Report*; The National Acadamies Press: Washington, DC, USA, 2004.
11. Ellingson, R.G.; Yanuk, D.J.; Lee, H.-T.; Gruber, A.A. Technique for estimating outgoing longwave radiation from HIRS radiance observations. *J. Atmos. Ocean. Technol.* **1989**, *6*, 706–711. [CrossRef]
12. Ellingson, R.G.; Lee, H.-T.; Yanuk, D.; Gruber, A. Validation of a technique for estimating outgoing longwave radiation from HIRS radiance observations. *J. Atmos. Ocean. Technol.* **1994**, *11*, 357–365. [CrossRef]
13. Lee, H.-T.; Gruber, A.; Ellingson, R.G.; Laszlo, I. Development of the HIRS outgoing longwave radiation climate dataset. *J. Atmos. Ocean. Technol.* **2007**, *24*, 2029–2047. [CrossRef]
14. NOAA Polar Orbiter Data (POD) User's Guide: 1998 Version. Available online: https://www1.ncdc.noaa.gov/pub/data/satellite/publications/podguides/TIROS-N%20thru%20N-14/pdf/NCDCPD-ch1.pdf (accessed on 2 August 2018).
15. NOAA KLM User's Guide: February 2009 Version. Available online: https://www1.ncdc.noaa.gov/pub/data/satellite/publications/podguides/N-15%20thru%20N-19/pdf/0.0%20NOAA%20KLM%20Users%20Guide.pdf (accessed on 2 August 2018).
16. Lee, H.-T. *Climate Algorithm Theoretical Basis Document (C-ATBD): Outgoing Longwave Radiation (OLR)—Daily*; CDRP-ATBD-0526; NOAA's Climate Data Record (CDR) Program: Ashveille, NC, USA, 2014.
17. Ba, M.B.; Ellingson, R.G.; Gruber, A. Validation of a technique for estimating OLR with the GOES sounder. *J. Atmos. Ocean. Technol.* **2003**, *20*, 79–89. [CrossRef]
18. Lee, H.-T.; Heidinger, A.; Gruber, A.; Ellingson, R.G. The HIRS outgoing longwave radiation product from hybrid polar and geosynchronous satellite observations. *Adv. Space Res.* **2004**, *33*, 1120–1124. [CrossRef]
19. Kondratovich, V. *GOES Surface & Insolation Products (GSIP)*; version 3.3; National Environmental Satellite, Data, and Information Service, Office of Satellite Data Processing and Distribution: College Park, MD, USA, 2013.
20. Lee, H.-T.; Laszlo, I.; Gruber, A. *Algorithm Theoretical Basis Document (ATBD): ABI Earth Radiation Budget—Outgoing Longwave Radiation*; NOAA NESDIS Center for Satellite Applications and Research (STAR): College Park, MD, USA, 2010.
21. Knapp, K.R.; Ansari, S.; Bain, C.L.; Bourassa, M.A.; Dickinson, M.J.; Funk, C.; Helms, C.N.; Hennon, C.C.; Holmes, C.D.; Huffman, G.J.; et al. Globally gridded satellite observations for climate studies. *Bull. Am. Meteorol. Soc.* **2011**, *92*, 893–907. [CrossRef]
22. Lee, H.-T. *Climate Algorithm Theoretical Basis Document (C-ATBD): Outgoing Longwave Radiation (OLR)-Monthly*; CDRP-ATBD-0097; NOAA's Climate Data Record (CDR) Program: Asheville, NC, USA, 2017.
23. Knapp, K.R. Scientific data stewardship of international satellite cloud climatology project B1 global geostationary observations. *J. Appl. Remote Sens.* **2008**, *2*, 023548. [CrossRef]
24. Gruber, A.; Ellingson, R.; Ardanuy, P.; Weiss, M.; Yang, S.K.; Oh, S.N. A Comparison of ERBE and AVHRR Longwave Flux Estimates. *Bull. Am. Meteorol. Soc.* **1994**, *75*, 2115–2130. [CrossRef]

25. Kiladis, G.N.; Straub, K.H.; Haertel, P.T. Zonal and vertical structure of the Madden–Julian oscillation. *J. Atmos. Sci.* **2005**, *62*, 2790–2809. [CrossRef]
26. Kiladis, G.N.; Wheeler, M.C.; Haertel, P.T.; Straub, K.H.; Roundy, P.E. Convectively coupled equatorial waves. *Rev. Geophys.* **2009**, *47*, RG2003. [CrossRef]
27. Schreck, C.J.; Shi, L.; Kossin, J.P.; Bates, J.J. Identifying the MJO, equatorial waves, and their impacts using 32 years of HIRS upper-tropospheric water vapor. *J. Clim.* **2013**, *26*, 1418–1431. [CrossRef]
28. Bates, J.J.; Jackson, D.L.; Bréon, F.-M.; Bergen, Z.D. Variability of tropical upper tropospheric humidity 1979–1998. *J. Geophys. Res.* **2001**, *106*, 32271–32281. [CrossRef]
29. Lee, H.-T. *NOAA Climate Data Record (CDR) of Daily Outgoing Longwave Radiation (OLR)*, version 1.2; NOAA CDR Program: Asheville, NC, USA, 2014. [CrossRef]